Tracking of Extended Objects with High-Resolution Doppler Radar

Dominik Kellner, *Student Member, IEEE*, Michael Barjenbruch, *Student Member, IEEE*, Jens Klappstein, Jürgen Dickmann, and Klaus Dietmayer, *Member, IEEE*

***Abstract*—In an urban environment, one of the key challenges remains to be the reliable estimation of the other traffic participants' motion state. Due to the highly nonlinear motions in city traffic, an instant and precise estimation of heading direction, velocity, and, particularly, yaw rate is required. Radar sensors are well suited for this task due to their robustness to environmental influences and direct measurement of the radial (Doppler) velocity. High-resolution radars receive multiple reflections from an extended object. In comparison to state-of-the-art approaches, not only is the Doppler velocity of a single reference point taken into account, but also is the distribution of the Doppler velocity across the vehicle analyzed. The velocity profile is derived with characteristic features and a corresponding sample covariance. These are fused into an unscented Kalman filter, resulting in a significant accuracy improvement and a reduction in the latency of the filter to almost zero during a change in motion or initialization. This yields a great improvement in determining the trajectories of potential critical objects, increasing the time to avoid collisions. Furthermore, the approach enables simultaneous identification of the rotation center of the object, which is essential for the tracking of highly dynamic maneuvers. All approaches were implemented and evaluated on a large experimental data set using highly precise reference systems as ground truth. The results show an impressive improvement in the accuracy of the yaw rate estimation of a factor of 3–4 compared with state-of-the-art approaches in a dynamic scenario.**

***Index Terms*—Doppler radar, tracking, motion estimation, collision avoidance, radar signal processing, intelligent vehicle.**

I. Introduction

ONE of the key challenges for future Advanced Driver Assistance Systems (ADAS) up to Fully Automated Driving will be the detection and interpretation of hazardous situations in an urban environment. A crucial task is the determination of the motion state of other traffic participants. In contrast to highways scenarios, where mainly linear motion and a low yaw rate exist, the dynamic of movements is increased in city traffic. The yaw rate and its fluctuation are significantly higher in dynamic scenarios such as turns, roundabouts, merging and intersections. Further, in highway scenarios traffic participants occur only longitudinally to the driving direction. In contrast, city scenarios also have them appearing laterally or from a temporary occlusion. This reduces the time to react to a potentially critical situation. A fast and reliable estimation of the full object motion state, including precise yaw rate estimation is therefore essential for future applications.

Doppler radar sensors are extremely well-suited to this task, providing direct measurement of the radial (Doppler-) velocity, a high accuracy in range and robustness to different weather conditions [1]. Not only the segmentation and association task is simplified using the Doppler information, but high lateral and rotational acceleration can be resolved. Due to an increasing measurement resolution in all dimensions, more than one reflection (referred to as detection) is received of an extended object (referred to as target).

In this paper, the problem of tracking extended targets with multiple radar detections is considered. The detections are not necessarily the contour of the vehicle and their relative positions to the vehicle cannot be reliably estimated. A precise determination of the orientation and contour of the vehicle is not feasible, so that the spatial extension is reduced to a single representation point. By tracking this point, a systematic error in velocity, heading and turn rate is injected during a nonlinear motion if the representation point is not at the rotation center or is not stable relatively to the target over consecutive frames.

To compensate an unstable representation point and to be able to detect and track even highly dynamic maneuvers, the velocity profile [2] is integrated into the tracking algorithm. By extracting the sinusoidal progress of the Doppler velocity over the azimuth angle (kinematic extension), precise information on the motion state is obtained. By comparing the position derivation of the representation point over consecutive frames (heading, turn rate & velocity) with the motion parameters of the velocity profile, the tracking algorithm is able to determine the rotation center of the extended target without any spatial information. A precise determination of the motion state of an extended target is only possible with knowledge of the rotation center [3].

The main contributions of this paper are the integration of the kinematic extension into dynamic extended object tracking. State of the art approaches integrate only the Doppler velocity of a single detection. An online estimation of the rotation center is performed without any model assumptions directly in the tracking filter. State of the art approaches use a spatial vehicle

Manuscript received June 22, 2015; revised September 18, 2015; accepted November 15, 2015. Date of publication December 17, 2015; date of current version April 29, 2016. The Associate Editor for this paper was J. M. Alvarez.

D. Kellner, M. Barjenbruch, and K. Dietmayer are with the driveU/Institute of Measurement, Control and Microtechnology, Ulm University, 89081 Ulm, Germany (e-mail: dominik.kellner@uni-ulm.de).

J. Klappstein and J. Dickmann are with Group Research and Advanced Engineering, Daimler AG, 89081 Ulm, Germany.

Color versions of one or more of the figures in this paper are available online at http://ieeexplore.ieee.org.

Digital Object Identifier 10.1109/TITS.2015.2501759

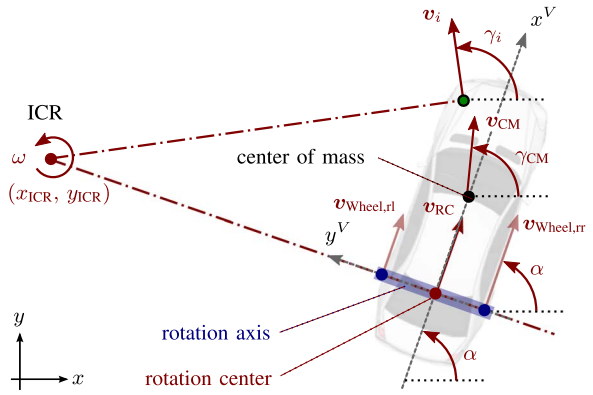

Fig. 1. Motion state of an extended target with the velocity vector $\boldsymbol{v}$ at different positions on the vehicle, the orientation α, heading γ_i and instant center of rotation (ICR) at a drift-free driving state.

model to determine the rear axle of the vehicle and use this as rotation center, with the assumption of a drift free driving state. Therefore the fit of a bounding box and the assumption that the rotation center is always at the rear axle of the vehicle are not required. This enables a tracking even in highly dynamic scenarios.

The paper is structured as follows. In Section II, the motion state of an extended target is described and definitions of terms used in this paper are given. Related work is reviewed in Section III and illustrated on a sequence captured with different automotive radars. The kinematic extension is examined in Section IV, and with the velocity profile parameters, a representation of it is derived. Section V concerns the integration of these parameters in a tracking algorithm, whereas Section VI extends it to an extended object tracking by an estimation of the rotation center of the vehicle. Experimental results on a large data set containing ground truth information are shown in Section VIII. All newly developed methods are examined and compared with state of the art approaches using a pre-series and experimental radar sensor.

II. Motion Description

A. Motion State

The complete 2 dimensional motion state $\boldsymbol{m}$ with 3 degrees of freedom (DOF) of an extended target can be fully described by the velocity vector $\boldsymbol{v}_p$ and yaw rate ω at an arbitrary representation point p: $\boldsymbol{m}_p = [v_p^x \; v_p^y \; \omega]^\intercal$, as shown in Fig. 1. The yaw rate is independent of the position and is equal to the change of the orientation α of the target over time $\omega = \partial\alpha/\partial t$. The representation point does not necessarily have to be on the vehicle. For clarity, the corresponding velocity vector is referred to virtual in such a case. In general, the motion state $\boldsymbol{m}_p$ can be transformed from a point p to a point q with the following transformation $\boldsymbol{T}_{p,q}$:

$$\underbrace{\begin{bmatrix} \omega \\ v_q^x \\ v_q^y \end{bmatrix}}_{\boldsymbol{m}_q} = \underbrace{\begin{bmatrix} 1 & 0 & 0 \\ -(y_q - y_p) & 1 & 0 \\ (x_q - x_p) & 0 & 1 \end{bmatrix}}_{\boldsymbol{T}_{p,q}} \underbrace{\begin{bmatrix} \omega \\ v_p^x \\ v_p^y \end{bmatrix}}_{\boldsymbol{m}_p}. \quad (1)$$

Knowing the covariance matrix of the motion state $\boldsymbol{\Sigma}(\boldsymbol{m}_p)$, the matrix can be transformed according to [4] at point q:

$$\boldsymbol{\Sigma}(\boldsymbol{m}_q) = \boldsymbol{T}_{p,q} \cdot \boldsymbol{\Sigma}(\boldsymbol{m}_p) \cdot (\boldsymbol{T}_{p,q})^\intercal. \quad (2)$$

B. Definitions

In this section, some definitions are introduced. The definitions are valid for an urban scenario with a velocity < 20 m/s and highly dynamic maneuvers up to 60°/s. For highway scenarios, in most cases, the yaw rate is small, so that the effects discussed in this section have a negligible influence.

- **Orientation α and heading γ_i**
  The orientation α of the vehicle is defined as the orientation of the longitudinal vehicle's axis x^V, which is orthogonal to the rear axle of the vehicle y^V. In comparison, the heading γ_i is the direction of movement of each point i on the vehicle, which can vary during a turn maneuver ($\omega \neq 0$), as shown in Fig. 1.
- **Instant Center of Rotation (ICR)**
  For a rigid body, the ICR is the stationary point (virtual velocity is zero) about which the body is instantaneously rotating. Equation system (1) can be used to find the point $(x_{\mathrm{ICR}}, y_{\mathrm{ICR}})$ where the corresponding velocity vector is zero ($\boldsymbol{v}_{\mathrm{ICR}} \stackrel{!}{=} 0$).
- **Drift-Free Driving State**
  In this paper, a drift-free driving state refers to a motion state without any lateral drift at the rear wheels (Fig. 1). The heading direction of the rear wheels $\gamma_{\mathrm{Wheel,r}}$ is then parallel to the vehicle's orientation α.
- **Rotation Axis (RA)**
  The rotation axis is the set of points on the target for which the heading γ_i is parallel to the vehicle's orientation α during a turning maneuver ($\omega \neq 0$). This is equivalent to the straight line from the ICR to the rotation center, which is orthogonal to the vehicle's orientation. This axis is equal to the rear axle at a drift-free driving state. If lateral drift takes place at the rear wheels, the rotation axis is shifted, typically forward in the driving direction (oversteering).
- **Rotation Center (RC)**
  The rotation center is the only point on the vehicle where the yaw rate and velocity are completely decoupled. The rotation center is the point on the rotation axis, which absolute velocity is constant during a change of the yaw rate ($|\partial\omega/\partial t| > 0$) at constant speed. At a drift-free driving state, it is equal to the center of the rear axle.

The local vehicle coordinate system is defined at the center of the rear axle with the x^V-axis pointing in the driving direction. The velocity vector $\boldsymbol{v}_{\mathrm{RC}}^V$ at the rotation center is reduced to a x^V-component $v_{\mathrm{RC}}^{V,x}$, while $v_{\mathrm{RC}}^{V,y}$ is zero, since the rotation axis is always parallel to the x-axis of vehicle's coordinate system. For a drift-free driving state, $(x_{\mathrm{RC}}^V, y_{\mathrm{RC}}^V)$ is zero. The velocity

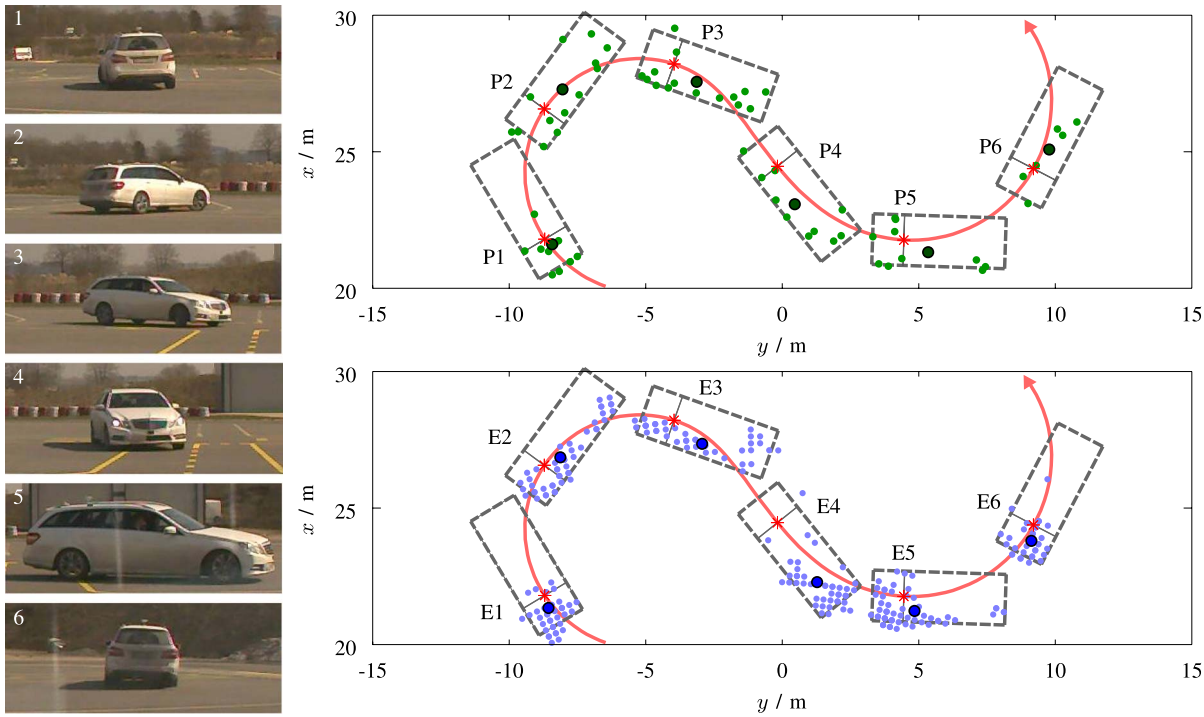

Fig. 2. Example measurements of a half a figure eight, resolved by a pre-series radar (top—green) and experimental radar (bottom—blue) with the average position of all detections (large •) and ground truth position of the vehicle (gray - - -) and ground truth trajectory (red).

vector $\boldsymbol{v}_i^V$ of each point is calculated using (1) in the vehicle's coordinate system:

$$\boldsymbol{v}_i^V = \begin{bmatrix} v_{\mathrm{RC}}^{V,x} - \omega \cdot \left(y_i^V - y_{\mathrm{RC}}^V\right) \\ \omega \cdot \left(x_i^V - x_{\mathrm{RC}}^V\right) \end{bmatrix}. \tag{3}$$

During a linear motion all points have the same velocity vector. For a turning maneuver, the velocity vector of points on the rotational axis (excluding the rotation center) have a different longitudinal velocity $v_i^{V,x}$. For all other points, the lateral velocity $v_i^{V,y}$ changes in addition. The velocity vector can be transformed into the global coordinate system using orientation α. The heading γ_i for any point can be calculated:

$$\gamma_i = \arctan\left(\frac{\omega \cdot \left(x_i^V - x_{\mathrm{RC}}^V\right)}{v_{\mathrm{RC}}^{V,x} - \omega \cdot \left(y_i^V - y_{\mathrm{RC}}^V\right)}\right) + \alpha. \tag{4}$$

Again, for a linear motion, all points on the vehicle have the identical heading α. With an increasing yaw rate, the deviation of the heading increases with a larger distance from the rotation center. For points on the rotation axle $(y_i^V - y_{\mathrm{RC}}^V)$, the additional angle is zero, and therefore, $\gamma_i = \alpha$.

III. Related Work

A. Extended Object Tracking With Doppler Radar

There are two main approaches to deal with multiple detections on an extended target. Both are discussed on a sample scene of a turning car with a pre-series and experimental 77 GHz Doppler radar (Fig. 2). The first approach reduces the spatial extension to a single representation point, which is the average position of all detections (referred to as average detection) or the closest detection to the sensor. Besides the loss of information about the target orientation, the representation point is not necessarily stable. In Fig. 2 at position E1, the average detection is behind the rear axle and then moves almost to the front (E4) and again back to the rear part of the vehicle until E6. The average and closest detection change their relative position to the vehicle due to measurement uncertainty, partial occlusions and a changing aspect angle. By using the closest point, a heuristic has to be added to compensate situations where it is not stable, e.g., for a crossing vehicle, it moves from the front to the rear part of the vehicle.

The second approach is an extended object tracking, where the spatial extension is taken into account by fitting an appropriate geometric model analog to laser scanner (e.g., a bounding box) [5] or using a radar response model [1], [6]–[8]. This spatial representation is now tracked over multiple frames by taking its position and orientation into account. First attempts are made to extract a geometric model of the vehicle by fitting a rectangle [5] independent of reflection centers and model assumptions. It shows promising results on real world examples with 50% of the measurements with an orientation error smaller than 3°. However, the approach mispredicts (up to 45°) when only a single reflection center is resolved or reflection centers are blurred. For example, if only the front or rear part is visible (E1, E6, P6), it is obvious that any approach taking only the spatial extension into account would fail. Since it is hard to detect these outliers in the orientation estimation as well as calculating an appropriate sample covariance of the parameters, a reliable estimation is not yet applicable for a tracking algorithm.

Another way is to use a radar response model to associate detections to a relative position on the target. Radar response models use a discrete set of reflection centers, which are

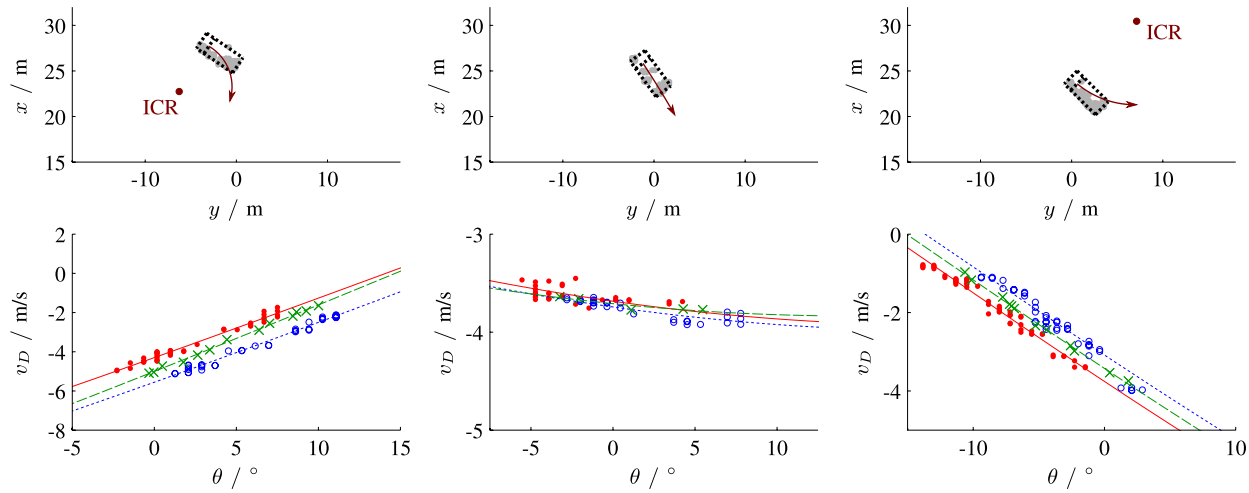

Fig. 3. Three example measurements of a vehicle changing from a right into a left turn from the sample sequence in Fig. 2; Received detections and instantaneous estimation of the motion state (red) (1. row) and velocity profiles of two experimental radar sensors (left sensor: red — with measurements •, right sensor: blue ··· with measurements ○) and a single pre-series radar (green - - - with measurements x).

resolved from the radar sensor under several assumptions like the form of the contour, the angle of incidence and material. These vehicle specific models are either designed for simulation purposes [6] or underlie large [1], [7]. The last two suffer from the difficult task of an association of detections to possible reflection centers. The model is rather simple, neither detections on the underbody of the vehicle are modeled, nor the case when the sensor is orthogonal to a plane (e.g., a side of the vehicle). Micro Doppler measurements of the wheels with a wrong Doppler velocity are not excluded. For example, in P6, only one out of seven detections lies on the contour, the rest come from the underbody. In P2, eight detections are captured on the side of the vehicle, and in P1, six detections on the rear part of the vehicle. In both situations, radar response models [6] and [8] would expect only two detections.

The main drawback of these models is that none takes the Doppler resolution into account. Due to different aspect angles and during a turning maneuver, the Doppler velocity can vary up to 5 m/s and even more (see Fig. 3-right). Detections are resolved since they fall into different Doppler cells (Doppler resolution is on the order of 0.1–0.3 m/s), which makes these models unsuitable for tracking moving vehicles.

Since the rotation center cannot be extracted from the spatial extension without any model assumptions, this paper reduces the spatial extension to a single representation point (average detection). In contrast, the kinematic extension is analyzed to obtain precise motion estimation.

B. Doppler Integration of Radar

Tracking objects in dynamic maneuvers (acceleration, yaw acceleration) using the measured Doppler velocity is challenging, since it is a superpositioning of the translation and rotational movement (eq. (3)). Further, the target dynamics are usually modeled in a Cartesian coordinate system, while the measurements are available in the polar coordinate system of the sensor.

To overcome a highly nonlinear update step for a Cartesian state space, the Doppler velocity is usually not used directly [9]. Conversion techniques can be applied to treat the range rate as a linear measurement in Cartesian coordinates [10] or a sequential *Unscented Kalman Filter (UKF)* is used, which updates the range rate in a pseudo measurement decoupled of the position update [11]. Further, the Doppler velocity is used to detect maneuvers and adjust the noise parameters of the tracking [9] or is integrated in an Interacting Multiple Model Filter (IMM) to switch between less and high dynamic models [10], [12], [13]. As a maneuver indicator, the range-Doppler profile of an extended target is analyzed [14]. In a single range cell, multiple Doppler velocities (kinematic extension) are measured, when a nonlinear movement is present. A direct relation to the motion parameters is only possible with model assumptions (width, orientation angle and turning direction).

In contrast, this paper analyzes the kinematic extension over the azimuth angle (velocity profile), since a direct relation to the motion state of the vehicle can be derived. An example for the velocity profile of the car in Fig. 2 changing from a right to a left turn is shown in Fig. 3. It is clearly visible that the velocity profile changes its gradient directly after the change of the turning direction. Without taking the range into account, a possible correlation of range and Doppler velocity has no influence [15]. Further, by using a chirp-sequence modulation the correlation is small already, due to extremely short chirp duration. The results are two motion parameters in Cartesian coordinates for each sensor, describing the motion of the target. Thus, a nonlinear transformation from polar measurement space to Cartesian space is not required for the range rate measurements.

C. Rotation Center

One of the most significant problems in extended object tracking with automotive radars is the uncertain measurement model [13]. The detections move dependent on the aspect angle

and reflection centers relative to the target. Therefore, it is important, that the displacement of a representation point to the rotation center is estimated. Otherwise a deviating representation point leads to a significant prediction error of rotational movements and directly impacts the resulting motion parameter estimates [3].

The problem is described in detail for an extended object tracking using stereo images [3] and video sequences [16]. The difference between the local target coordinate system and the rotation center is modeled with 3 DOF (translation + orientation) in the global coordinate system. [3] states that the estimated velocity vectors of the extracted features, determined by sparse scene flow, are not sufficient for estimating the rotation center. It is assumed that the center of the rear axle is the rotation center, which limits the approach to a drift-free driving state. Since the axle cannot be determined directly, a cuboid model is fitted and a constant distance from the rear part is used to estimate the rear axle. This is challenging for approaching targets, where only the front is visible. Further, the three parameters are included in the tracking filter and updated at each time step.

Two Doppler radars are used to track other vehicles in a highway scenario in [13]. A drift-free driving state is assumed and only a single detection is received of each target. An IMM algorithm using extended Kalman filters (IMM/EKF) is used, taking the position and Doppler velocity into account. In total four motion models and 12 measurement models, describing different locations of the received detection (on the side and corner of the vehicle), are used. The width and length of the target are predetermined in advance and it is assumed that the detection is always at the boundary of the target. If the average detection moves relative to the target, e.g., due to a changing aspect angle, an occurring error is compensated by a model switch. Further, the rotation center is assumed to be at the mass center of the vehicle and that no lateral velocity component is present at this position. Therefore, a systematic error is induced during a turning maneuver (drift-free driving state), since the rotation center is at the rear axle as explained in Section II-B.

In this paper, however, the rotation center is determined solely through a comparison of the movement of an arbitrary representation point with the kinematic extension. Therefore no spatial assumptions about the target size and rear axle or rotational axes are required and so even a lateral drift of the target can be resolved. The rotation center is integrated directly in the Kalman Filter in the local target coordinate system. This reduces the required additional states from three to two (relative displacement in vehicle coordinate system). An additional modification using the rotation axis reduces the required states to a single additional state. In both cases, even if the rotation center is obscured or outside the field of view, an estimation is archived without any model assumptions.

IV. Kinematic Extension (Velocity Profile)

Instead of using the Doppler velocity of a single or multiple detections directly, the velocity profile (Doppler velocity over azimuth angle) with a representation in Cartesian space is derived. The velocity profile of a single sensor is then extended to multiple sensors, assuming the ego-vehicle stands still (ego-vehicle and global coordinate system are identical). In the last step, modifications are derived for a non-stationary ego-vehicle.

A. Single Sensor

A high-resolution Doppler radar receives more than one detection i of an extended target. It measures the azimuth angle θ_i^S in the sensor coordinate system S, distance r_i and radial Doppler velocity $v_{D,i}$ of each detection. For the transformation in the ego-vehicle coordinate system only θ_i^S has to be compensated by the mounting orientation of the sensor. Then the Cartesian position (x_i, y_i) can be calculated using θ_i and r_i and the sensor position (x_S, y_S). The measured Doppler velocity corresponds to the radial velocity component of the detection's motion state $\boldsymbol{m}_i = [\omega, v_i^x, v_i^y]^\intercal$:

$$v_{D,i} = \begin{bmatrix} 0 & \cos(\theta_i) & \sin(\theta_i) \end{bmatrix} \cdot \boldsymbol{m}_i. \tag{5}$$

For an arbitrary representation point the transformation to the motion state of all detections $\boldsymbol{m}_i$ can be calculated using (1). The chosen representation point is the sensor position at the ego-vehicle $\boldsymbol{m}_S$, which will be motivated later. The motion state at the detection in (5) is now determined from the virtual motion state $\boldsymbol{m}_S$ using $\boldsymbol{T}_{S,i}$ from (1):

$$v_{D,i} = \begin{bmatrix} 0 & \cos(\theta_i) & \sin(\theta_i) \end{bmatrix} \cdot \boldsymbol{T}_{S,i} \cdot \boldsymbol{m}_S \tag{6}$$

which after multiplying results in:

$$v_{D,i} = (v_S^x - \omega(y_i - y_S))\ \cos(\theta_i) + (v_S^y + \omega(x_i - x_S))\ \sin(\theta_i). \tag{7}$$

The result is a cosine equation with 2 parameters (phase shift and amplitude) but 3 DOF ($\boldsymbol{m}_S$). In general even with more than three detections it is not possible to resolve the complete motion state. The motivation for the choice of the sensor's position as reference point gets obvious, when replacing the relative position x_i and y_i by their polar representation $r_i \cos(\theta_i) + x_S$ respectively $r_i \sin(\theta_i) + y_S$. Thus, the ω components are eliminated in (7) resulting in an equation with 2 DOF:

$$v_{D,i} = v_S^x \cdot \cos(\theta_i) + v_S^y \cdot \sin(\theta_i). \tag{8}$$

The solution of the equation is denoted as the *Velocity Profile* of a single sensor. It is decoupled of the exact position of the detection in relation to the sensor, but as well to its relative position on the target. Two detections under a deviating angle are sufficient to determine the two parameters $\boldsymbol{v}_S$, but with more detections using a regression calculation the accuracy is improved:

$$\min_{v_S^x, v_S^y} \left\| \begin{bmatrix} \cos(\theta_1) & \sin(\theta_1) \\ \vdots & \vdots \\ \cos(\theta_N) & \sin(\theta_N) \end{bmatrix} \cdot \begin{bmatrix} v_S^x \\ v_S^y \end{bmatrix} - \begin{bmatrix} v_{D,1} \\ \vdots \\ v_{D,N} \end{bmatrix} \right\|_2^2. \tag{9}$$

It is possible to estimate the velocity vector $\hat{\boldsymbol{v}}_S$ by a simple Least-SQuare (LSQ) regression, but due to the measurement uncertainty in the dependent $v_{D,i}$ as well as independent variables θ_i the result is biased. This problem is called

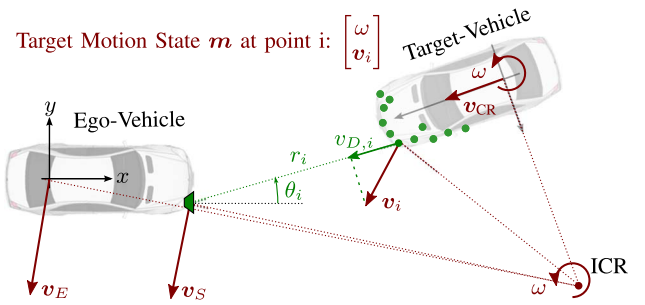

Fig. 4. Target motion state $\boldsymbol{m}$ (red) at different representation points. Velocity vector at the target vehicle's center of rear axis $\boldsymbol{v}_{\mathrm{CR}}$, center of rear axis of the ego-vehicle $\boldsymbol{v}_E$, sensor position $\boldsymbol{v}_S$ and ICR - Instant Center of Rotation ($\boldsymbol{v}_{\mathrm{ICR}} := 0$). The radar measures of each detection i the radial distance r_i, the Doppler velocity $v_{D,i}$ and the azimuth angle θ_i in ego-vehicle coordinate system (green).

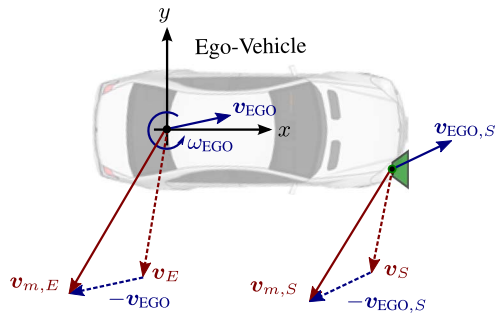

Fig. 5. Measured virtual velocity vectors $\boldsymbol{v}_{m,E}$ and $\boldsymbol{v}_{m,S}$ of Fig. 4, when the ego-vehicle is moving with a yaw rate ω_{EGO} and a velocity vector $\boldsymbol{v}_{\mathrm{EGO}}$ at the center of the rear axis and the ego-motion compensated velocity vectors $\boldsymbol{v}_E$ and $\boldsymbol{v}_S$.

Errors-in-variables (EIV) [17] and the maximum likelihood estimator is an *Orthogonal-Distance-Regression* (ODR) [18]. The algorithm and the determination of the corresponding sample covariance matrix are described in detail in [2]. The representation of the velocity profile for a later integration in the Kalman Filter is the estimated velocity $\tilde{\boldsymbol{v}}_S$ and an estimate of the corresponding covariance $\mathrm{cov}(\tilde{\boldsymbol{v}}_S)$.

B. Multiple Sensors

As derived in the previous section, a single radar is able to resolve 2 DOF of the motion state. With at least two radar sensors $j = 1 \dots M$ resolving detections on the same target (in total 3 or more), it is possible to determine the complete motion state in a single measurement. Therefore, the choice of the representation point is not further restricted to the sensor position. The *Instant Center of Rotation* (ICR) is determined by finding the point, where the velocity vector is zero [2]. For later use in a tracking algorithm and for a simple compensation of the ego-motion, the center of the rear axle of the ego-vehicle (E) is used as the representation point. All representation points are shown in Fig. 4. The equation can be set up for each target, analog to (7):

$$v_{D,j,i} = (v_E^x - \omega\, y_i)\ \cos(\theta_{j,i}) + (v_E^y + \omega\, x_i)\ \sin(\theta_{j,i}) \tag{10}$$

and after replacing the target positions (x_i, y_i) analog to (8):

$$v_{D,j,i} = (v_E^x - \omega\, y_{S,j})\ \cos(\theta_{j,i}) + (v_E^y + \omega\, x_{S,j})\ \sin(\theta_{j,i}). \tag{11}$$

An equation system is set up using all detections of all radar sensors:

$$\min_{\boldsymbol{m}_E} \left\| \begin{bmatrix} \chi_{1,1} & \cos(\theta_{1,1}) & \sin(\theta_{1,1}) \\ \vdots & \vdots & \vdots \\ \chi_{1,N} & \cos(\theta_{1,N}) & \sin(\theta_{1,N}) \\ \vdots & \vdots & \vdots \\ \chi_{M,1} & \cos(\theta_{M,1}) & \sin(\theta_{M,1}) \\ \vdots & \vdots & \vdots \\ \chi_{M,N} & \cos(\theta_{M,N}) & \sin(\theta_{M,N}) \end{bmatrix} \begin{bmatrix} \omega \\ v_E^x \\ v_E^y \end{bmatrix} - \begin{bmatrix} v_{D,1,1} \\ \vdots \\ v_{D,1,N} \\ \vdots \\ v_{D,M,1} \\ \vdots \\ v_{D,M,N} \end{bmatrix} \right\|_2^2 \tag{12}$$

with $\chi_{j,i} = -y_{S,j}\cos(\theta_{j,i}) + x_{S,j}\sin(\theta_{j,i})$.

The following estimation is identical to the previous section and the motion parameter $\boldsymbol{m}_E$ and sample covariance matrix $\mathrm{cov}(\boldsymbol{m}_E)$ are determined using ODR. With the full motion state of the target vehicle, the velocity vector of each detection can be estimated:

$$\boldsymbol{m}_i = \boldsymbol{T}_{E,i} \cdot \boldsymbol{m}_E. \tag{13}$$

C. Ego-Motion Compensation

In the last two sections a stationary ego-vehicle was assumed. When the ego-vehicle moves, its motion state $\boldsymbol{m}_{\mathrm{EGO}}$ can be described by a yaw rate ω_{EGO} and velocity vector at the center of the rear axle $\boldsymbol{v}_{\mathrm{EGO}}$ as shown in Fig. 5. In addition to the motion state the corresponding ego-motion covariance matrix $\mathrm{cov}(\boldsymbol{m}_E)$ is determined, e.g., by the inertial sensors' specifications. The ego-motion state at any position p of the vehicle $\boldsymbol{v}_{\mathrm{EGO},p}$ can be calculated analog to (1). When the ego-vehicle approaches a target, from the sensors' points of view the target moves towards the sensor, resulting in an additional negative Doppler velocity. As a consequence the measured virtual motion $\boldsymbol{v}_{m,p}$ consists of the virtual motion vector $\boldsymbol{v}_p$ and the negative ego-motion at this point $\boldsymbol{v}_{\mathrm{EGO},p}$. Hence, the ego-motion has to be added to compensate the ego-vehicle movement. The same holds for the yaw rate. For the sensor motion vector $\boldsymbol{v}_S$ of (9) this yields:

$$\boldsymbol{v}_S = \boldsymbol{v}_{C,S} + \begin{bmatrix} 0 & 1 & 0 \\ 0 & 0 & 1 \end{bmatrix} \cdot \boldsymbol{T}_{E,S} \cdot \boldsymbol{m}_{\mathrm{EGO}} \tag{14}$$

and for the full motion state of (12):

$$\boldsymbol{m}_E = \boldsymbol{m}_{m,E} + \boldsymbol{m}_{\mathrm{EGO}}. \tag{15}$$

This motivates the choice of the ego-vehicle's rear axle as a representation point for the target motion. The ego-motion with the corresponding uncertainty can simply be added. For the virtual motion at the sensor position, the transformed approximated covariance matrix is used $(\boldsymbol{T}_{E,S}^{\intercal}\mathrm{cov}(\boldsymbol{m}_{\mathrm{EGO}})\boldsymbol{T}_{E,S})$.

V. Tracking Integration

In this section the estimated velocity profile parameters with their corresponding covariance matrix are included in a tracking

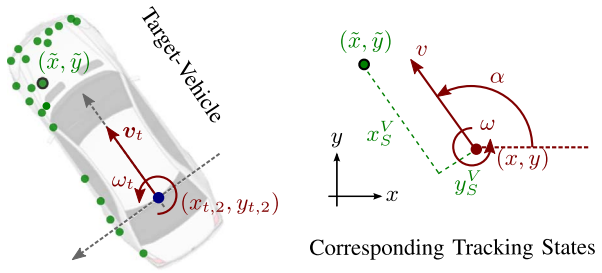

Fig. 6. Detections (green) and motion parameters (red) of a target (left) and the corresponding tracking states (right).

algorithm. The central focus here lies not on the tracking algorithm itself. Therefore, a UKF [19] is chosen for the tracking algorithm, due to the low computational complexity. It would also be possible to use a particle filter [20] or a combination of both (e.g., Rao-Blackwellized-Filter [21]) as tracking algorithm.

For simplification it is assumed that the ego-vehicle is standing still, so that the stationary global coordinate system is equivalent to the ego-vehicle coordinate system. The modifications for a moving ego-vehicle using an arbitrary stationary reference system are straightforward. The measurements are corrected by the current ego-vehicle position and orientation. The velocity profile is compensated by the ego-vehicle's motion as presented in Section IV-C. The compensation of the Doppler velocity is identical by compensating the radial velocity part caused by the sensor motion.

The notation of a state parameter is shorten to p (p_k), of predicted state estimates to $\hat{p}$ $(p_{k+1|k})$ and of measurements to $\tilde{p}$ $(\tilde{p}_k)$, where the k denotes the k-th time step.

A. Kalman Filter—State Vector

For a precise estimation of the trajectory of other traffic participants, a yaw rate estimation is essential. In critical maneuvers with a changing heading the trajectory of other traffic participants can be reliable determined (turning at intersections, entering/exit the roundabout, lane change procedure). The reason for that is that an estimate of the derivative of the heading exists with the yaw rate. Therefore, the *Standard Coordinate Turn Model (CT) with Polar Velocity* is chosen ([22, Section V-B]), assuming a constant turn rate and velocity.

The approach relies on target kinematics, by linking translation and rotational movement. The velocity is always along the heading direction. A lateral velocity orthogonal to the heading direction is not possible. It can solely be realized by rotating the heading direction $(|\omega| > 0)$.

The state vector of a classic position-based Kalman Filter (*PKF*) is in a stationary global coordinate system and has the following state parameters:

$$\boldsymbol{x}_{\mathrm{PKF}} = [x,\ y,\ \alpha,\ v,\ \omega]^{\mathsf{T}} \tag{16}$$

where the position is denoted by x and y, the heading direction with α, the velocity with v and the yaw rate with ω as illustrated in Fig. 6. The model implicitly assumes that the position refers to the center of rotation. A deviation causes a systematic error as discussed in the next section. The underlying dynamic model is nonlinear with the state transition matrix $\boldsymbol{x} = \boldsymbol{F}(\hat{\boldsymbol{x}})$. By using a constant turn ($\omega = \text{const.}$) and constant velocity model ($v = \text{const.}$), higher derivatives ($\dot{\omega}$ resp. $\dot{v}$) are realized by the additive white noise in the covariance matrix $\boldsymbol{Q}$ of the process model. They are specified by the standard deviation $\sigma_{\dot{\omega}}$ resp. $\sigma_{\dot{v}}$ and the effects are propagated on all entries of $\boldsymbol{Q}$.

It is essential that the reference coordinate system is stationary. The mentioned constraint does not hold for a moving reference coordinate system. For example, if the ego-vehicle follows the target vehicle with the identical velocity, a turning maneuver would result only in a lateral velocity. This is not possible due to the kinematic constraint, which is only valid in a stationary coordinate system.

B. Kalman Filter—Update Step

The update step is summarized in Table I with the measurement $\boldsymbol{z}$ and observation model $\boldsymbol{H}(\hat{\boldsymbol{x}})$. If multiple detections are received from an object, the average detection $(\tilde{x}, \tilde{y})$ is determined. The corresponding entries in the measurement covariance matrix $\boldsymbol{R}$ are difficult to determine. Beside the measurement noise of the radar sensor, an additional uncertainty has to be added. The reason for the additional uncertainty is that the filter state refers to the center of rotation, which is not always equal to the average detection. Therefore, the measurement uncertainty is determined experimentally and with a standard deviation of 1 m, has a larger uncertainty than the measurement uncertainty. In this section it is assumed that in average the measured position is equal to the rotation center.

The classic position-based Kalman Filter (*PKF-Pos*) has only the position $(\tilde{x}, \tilde{y})$ as measurement vector. The corresponding observation model is linear and does not depend on the current motion state. With an additional integration of the measured Doppler velocity, a more dynamic Kalman Filter (*PKF-vD*) is created. Through the velocity information, a derivative of the position is included so that braking and accelerating are faster determined. The observation model $\boldsymbol{H}(\hat{x})$ is highly nonlinear, since all state parameters are required to estimate the expected Doppler velocity. Another problem arises if multiple detections are received. The average Doppler velocity $\tilde{v}_D$ is calculated, which causes a small systematic error since the progress over the azimuth angle θ is not linear, but a sine as derived in (8).

The averaging of the Doppler velocities is improved through the integration of the velocity profile (*PKF-VP1*). For a single sensor the velocity profile is represented by the virtual velocity at the sensor position $\tilde{\boldsymbol{v}}_S$, determined by (9). Using a nonlinear transformation, the expected virtual velocity at the sensor position $\hat{\boldsymbol{v}}_S$ is determined out of the predicted state estimation $\hat{\boldsymbol{x}}_{\mathrm{PKF}}$. It is then compared in the innovation step with the measured parameters of the velocity profile. The corresponding covariance $\boldsymbol{\Sigma}(\tilde{\boldsymbol{v}}_S)$ is directly integrated in the corresponding entries of the measurement covariance matrix $\boldsymbol{R}$.

If multiple sensors receive detections from the same object, the full motion state of the object is estimated, represented by the virtual motion at the center of the ego-vehicle $\boldsymbol{m}_E$ (*PKF-VP2*). The predicted state estimation of the filter is transformed in this point $\hat{\boldsymbol{m}}_E$ and updated with the measurement $\tilde{\boldsymbol{m}}_E$. Alternatively, the determined motion state and the corresponding

TABLE I
OVERVIEW OF THE STATES AND MEASUREMENTS OF THE KALMAN FILTERS USING THE AVERAGE DETECTION

Tracker	$\boldsymbol{x}$	Filter	$\boldsymbol{z}_k$	$\boldsymbol{H}_{k+1}(\hat{\boldsymbol{x}}_{k+1\|k})$
Average Detection	$\begin{bmatrix} x \\ y \\ \alpha \\ v \\ \omega \end{bmatrix}$	*PKF-Pos*	$\begin{bmatrix} \tilde{x} & \tilde{y} \end{bmatrix}^\mathsf{T}$	$\begin{bmatrix} \hat{x} & \hat{y} \end{bmatrix}^\mathsf{T}$
		PKF-VD	$\begin{bmatrix} \tilde{x} & \tilde{y} & \tilde{v}_D \end{bmatrix}^\mathsf{T}$	$\begin{bmatrix} \hat{x} & \hat{y} & \frac{\hat{x}\hat{v}\cos(\hat{\alpha})+\hat{y}\hat{v}\sin(\hat{\alpha})}{\sqrt{\hat{x}^2+\hat{y}^2}} \end{bmatrix}^\mathsf{T}$
		PKF-VP1	$\begin{bmatrix} \tilde{x} & \tilde{y} & \tilde{v}_S^x & \tilde{v}_S^y \end{bmatrix}^\mathsf{T}$	$\begin{bmatrix} \hat{x} & \hat{y} & -\hat{\omega}\,(\hat{y}-y_S)+\hat{v}\cos(\alpha) & \hat{\omega}\,(\hat{x}-x_S)+\hat{v}\sin(\alpha) \end{bmatrix}^\mathsf{T}$
		PKF-VP2	$\begin{bmatrix} \tilde{x} & \tilde{y} & \tilde{v}_t^x & \tilde{v}_t^y & \tilde{\omega} \end{bmatrix}^\mathsf{T}$	$\begin{bmatrix} \hat{x} & \hat{y} & \hat{v}\cos(\hat{\alpha})-\hat{\omega}\hat{y} & \hat{v}\sin(\hat{\alpha})+\hat{\omega}\hat{x} & \hat{\omega} \end{bmatrix}^\mathsf{T}$

covariance matrix can be transformed into the position of the filter by a nonlinear transformation. Then the filter states can be updated directly. A standard (linear) Kalman Filter would then be sufficient.

C. Initialization

For the initialization of *PKF-Pos* and *PKF-VD*, a *Two-Point Differencing* (*2P-Initialization*) is used as described in detail in [23]. The initialization is performed after the second measurement $(\tilde{x}_{t,1}, \tilde{y}_{t,1})$. The heading and velocity are calculated using the displacement vector between both measurements $\tilde{\boldsymbol{v}}_{t,1}$. A yaw rate initialization is not possible with two measurements. Systematic errors are injected if the measurements are not at the same relative position on the vehicle and if a nonlinear motion $(\omega \neq 0)$ is present.

With a single sensor using the velocity profile (*PKF-VP1*), full initialization is not possible in a single step. In a scenario in which only low yaw rates occur, like on a motorway, the yaw rate is assumed to be zero and the measured velocity at the sensor position $\tilde{\boldsymbol{v}}_S$ is identical to that of the detection $\boldsymbol{v}_t$. A second possibility is to take the velocity vector of the *2P-Initialization*, which is equal to the current velocity vector $\tilde{\boldsymbol{v}}_t$ at the track position. The yaw rate can then be estimated by comparing this velocity vector with the velocity profile. This is achieved by calculating a simple least square solution of the last two rows of the transformation of the velocity vector (1):

$$\min_{\boldsymbol{m}_E} \left\| \begin{bmatrix} -(y_S - \tilde{y}_{t,1}) \\ (x_S - \tilde{x}_{t,1}) \end{bmatrix} \omega - \begin{bmatrix} \tilde{v}_S^x - \tilde{v}_{t,1}^x \\ \tilde{v}_S^y - \tilde{v}_{t,1}^y \end{bmatrix} \right\|_2^2. \tag{17}$$

In all cases, it is difficult to initialize the corresponding process matrix $\boldsymbol{P}_k$. The position states underlie a systematic variation due to the relative position on the target, which has to be taken into account. The dynamic states suffer from a relative movement of the reference point on the target. Further, by calculating the velocity from the displacement only an approximation of the velocity vector is determined in case of a nonlinear motion.

The initialization of the complete motion state with two velocity profiles (PKF-V2) is possible. The estimated motion state $\tilde{\boldsymbol{m}}_E$ of (11) is transformed at the representation point (x, y) using (1). The sample covariance is as well transformed (eq. (2)), so that beside an instant estimate of the complete state vector $\boldsymbol{x}_0$, the process matrix $\boldsymbol{P}_0$ is determined.

VI. FEATURE TRACKING

With the assumption in the previous section that the average detection is equal to the rotation center, systematic errors can occur if this assumption is violated. In the event of a nonlinear motion $(\omega \neq 0)$ the heading and velocity state and during a yaw acceleration $(\dot{\omega} \neq 0)$ the yaw rate state are affected. The average detection depends on the aspect angle and moves relative to the target vehicle for a changing aspect angle. It is unlikely that the track position is always at the center of rotation, nor that the displacement is normally distributed around the rotation center. Therefore, the Kalman Filter is extended with states describing the displacement of the average detection to the rotation center.

In the following the identification of the center of rotation without any spatial assumptions (e.g., vehicle's width, length, position of rear axle etc.) is presented. Contrary to state-of-the-art approaches, the rotation center is not estimated by identifying the position of the rear axle using spatial assumptions, but by comparing the motion of the representation point with the kinematic extension. The state-of-the-art approaches have two disadvantages. First, it is difficult to identify the rear axle using radar, since fitting a radar response model or bounding box is not always possible and the position relative to the model has to be determined with assumptions. Second, the approach is limited to a drift-free driving state, assuming that the rear axle is equivalent to the rotation axis.

A. State Vector

The relative displacement of the center of rotation to the expected average detection (further called feature) is specified by (x_S^V, y_S^V) as shown in Fig. 6. In contrast [3] defines the displacement and rotation in the global coordinate system and has to add three more states. With the displacement relative to the target only two additional states (x_S^V, y_S^V) are added:

$$\boldsymbol{x}_{\text{FFKF}} = \left[x,\ y,\ \alpha,\ v,\ \omega,\ x_S^V,\ y_S^V\right]^\mathsf{T}. \tag{18}$$

The difference is that both are in the target vehicle coordinate system, which is rotated with α in respect to the global coordinate system. The observation model $\boldsymbol{H}$ for all filters changes only for the position states:

$$\begin{bmatrix} H_{k+1}(x) \\ H_{k+1}(y) \end{bmatrix} = \begin{bmatrix} \hat{x} + \hat{x}^V \cdot \cos(\hat{\alpha}) - \hat{y}^V \cdot \sin(\hat{\alpha}) \\ \hat{y} + \hat{y}^V \cdot \cos(\hat{\alpha}) + \hat{x}^V \cdot \sin(\hat{\alpha}) \end{bmatrix}. \tag{19}$$

To determine the center of rotation, a measurement of the motion state of the vehicle is required. Therefore, this modification

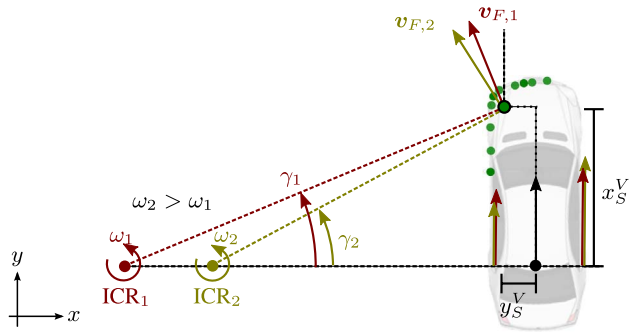

Fig. 7. Velocity vector $\boldsymbol{v}_F$ for the average detection on the vehicle (feature) and on the rotation axis for two different yaw rates ω_1 (red) and ω_2 (orange) (constant velocity).

cannot be applied to PKF-Pos, which would result in an ambiguity. The three other filters are modified and denoted as *FFKF-VD*, *FFKF-VP1* and *FFKF-VP2* (*FF* stands for the two new states).

A displacement in the lateral direction y_S^V does not induce a systematic error in the heading and yaw rate states, as shown in Fig. 7. Instead, the velocity has only a small deviation, with a maximum deviation of half of the vehicle's width multiplied by the yaw rate (e.g., width 2 m, $\omega = 50°/\text{s} \rightarrow \Delta v = 0.8$ m/s). The longitudinal displacement x_S^V on the other hand has a maximum value of the distance from the rear axle to the front which is approximately 3–4 m. By setting y_S^V to zero, a small systematic error in the velocity is injected, but the estimated filter states are reduced. The resulting filters with a single displacement in x_S^V are denoted with *FKF-VD*, *FKF-VP1* and *FKF-VP2*:

$$\boldsymbol{x}_{\text{FKF}} = \left[x,\ y,\ \alpha,\ v,\ \omega,\ x_S^V\right]^{\mathsf{T}}. \tag{20}$$

B. Displacement Process Noise

Since only the displacement (x_S^V, y_S^V) and not its deviation is included, a variation of the position is modeled by the covariance matrix of the process noise $\boldsymbol{Q}$. The maximum deviation of x_S^V is the vehicle length when the vehicle turns 180°, assuming that the feature is on the contour of the object. Further assumptions are a turning maneuver duration of 5 s and a vehicle length of 5 m. This results in a maximum displacement velocity $\dot{x}_S^V$ of 1 m/s. With an update rate of 15 Hz, the process noise of x_S^V is on the order of 0.005 m^2. The vehicle's width is approximately 2 m, so that the process noise of dy is on the order of 0.002 m^2.

The displacement is initialized to zero with very low process noise. The reason is that the displacement can only be determined when the vehicle changes its motion state, as discussed in detail in the next section. Therefore, if no motion state is available during the first measurements, x_S^V cannot be determined.

C. Observability

There are situations in which the displacement is unobservable. For example, during a linear motion all points on the vehicle have the identical velocity vector. A deviation in the yaw angle appears only during a nonlinear motion, as illustrated in Fig. 7:

$$\gamma_i = \alpha + \arcsin\left(\frac{\omega \cdot x_S^V}{|\boldsymbol{v}_F|}\right) \tag{21}$$

with $|\boldsymbol{v}_F|$ as absolute value of the velocity vector at the feature's position. The heading and absolute velocity can be determined by a tracking algorithm, whereas x_S^V and α cannot be resolved. ω can only be resolved using at least 2 radars. In all cases, the equation is overdetermined and an analytic solution of the displacement x_S^V is not available.

Therefore, consecutive measurements are required and the derivation of the heading has to be examined and compared with the Doppler information. An analysis of the observability can be realized by calculating the first derivation of (21):

$$\frac{\partial \gamma_i}{\partial t} = \omega + x_S \frac{\frac{\partial \omega}{\partial t}|\boldsymbol{v}_F| - \frac{\partial |\boldsymbol{v}_F|}{\partial t}\omega}{\sqrt{1 - \left(\frac{\omega \cdot x_S^V}{|\boldsymbol{v}_F|}\right)^2}}. \tag{22}$$

The displacement can only be determined if the second term is not equal to zero. The displacement is only observable if there is an acceleration $(\partial|\boldsymbol{v}_F|/\partial t \neq 0)$ during a turning maneuver $(\omega \neq 0)$ or there is a yaw acceleration $(\partial\omega/\partial t \neq 0)$. Both effects are equivalent to a displacement of the ICR. The sum is zero as well if the vehicle breaks and the yaw acceleration is negative or it accelerates and the yaw acceleration is positive in such a way, that the position of the ICR is constant.

VII. Experimental Results

A. Experimental Overview

All filters proposed in the last sections are evaluated on a large experimental data set (4500 measurements). A highly precise inertial measurement unit with DGPS support is used in both vehicles (position error < 2 cm), to get the exact relative position and ground truth motion parameters of the target vehicle. In this scene, the target vehicle drives in circles and eights in front of the ego-vehicle. The sequence is highly dynamic with an average absolute yaw rate of 45°/s and an average velocity of 8 m/s. The target vehicle varies in the distance from 15 m to 40 m (average 27 m).

The algorithm is real-time-capable with a computation time below 1 ms on an ordinary personal computer. The extension to multiple targets is straightforward since only the update step is modified. Thus, a state-of-the-art data association step can be applied.

The sequence is captured with an experimental radar and a pre-series radar, both operating at 77 GHz and with an update rate of 15 Hz. The experimental radar has an azimuth accuracy of 1° (interpolated) and a Doppler accuracy of 0.25 m/s and the pre-series radar has an azimuth accuracy up to 4° and a Doppler accuracy of 0.04 m/s.

Using the available ground truth, first a parameter sweep is performed on the complete sequence and an optimal parameterization is chosen for each filter. This is done by minimizing the

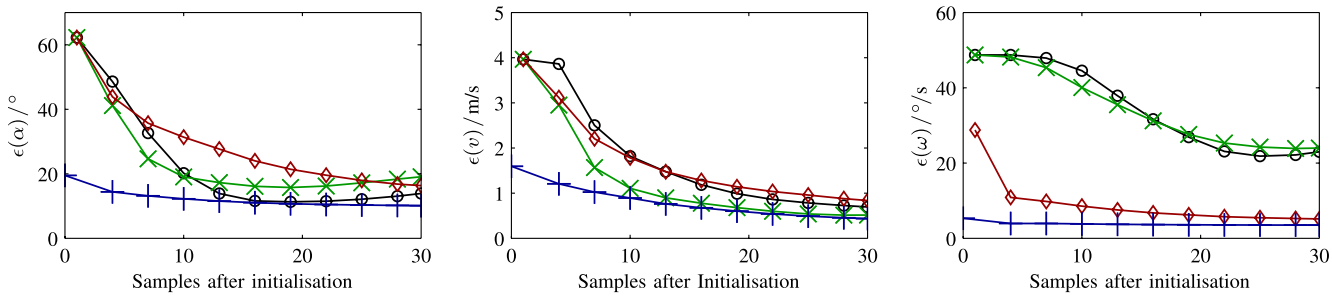

Fig. 8. RMSE for the heading (left), velocity (middle) and yaw rate (right) estimation at sample 0–30 (0–2 s) after initialization of 4470 tracks for *PKF-POS* (black—○), *PKF-VD* (green—x), *PKF-VP1* (red—◇) and *PKF-VP2* (blue—+).

sum of the state errors using its minimal value in all parameter sets. A crucial parameter is the additional process noise for the constant yaw rate $\sigma_{\dot{\omega}}$. If more information about the kinematic of the object is included in the filter, the optimal value decreases (*PKF-Pos*: 220°/s, *PKF-VD*: 110°/s, *PKF-VP1/VP2*: 28°/s). Since the reference point moves relative to the vehicle, this has to be taken into account in the measurement noise $\boldsymbol{R}$, which is significantly larger than the sensor's measurement accuracy. The parameter sweep determined the optimal value on the order of 0.5 m–1 m. The measurement uncertainty for the average Doppler measurement (*PKF-VD*) is determined to be 0.1 m/s.

A parameter sweep cannot be performed in a real application due to the missing reference system, but only in this manner can the best results be archived for each filter, making them comparable. The errors are analyzed in terms of *root-mean-squared error* (RMSE) and *median absolute deviation* (MAD). The MAD states that 50% of the absolute errors are below this value.

B. Initialization

The initialization approaches introduced in Section V-C are evaluated for the position based filters (*PKF-*). Since the displacement for the feature based filters are initialized with zero and a small process noise, there is almost no difference to the position based filters in the first two seconds. The initialization is performed for each measurement in the complete data set, assuming that the target has just appeared. The accuracy in terms of the RMSE over all 4470 initialization and the following two seconds are shown in Fig. 8. Since most of the time the motion state is nonlinear, it is equal to the initialization of a highly dynamic driving state.

Only the approach using two radar sensors (*PKF-VP2*) is able to estimate the filter states in a single measurement. Therefore, it is most accurate for all three dynamic states and its accuracy decreases only slightly with progressing time. For the orientation and velocity estimation, the RMSE of the other three filters are almost equal (Fig. 8-left & center). The filter using the Doppler information (*PKF-VD*) increases the initialization accuracy of the heading and velocity compared to the filter without any Doppler information (*PKF-POS*).

The major difference can be seen in the yaw rate estimation (Fig. 8-right). With the two-point initialization of *PKF-VP1* (eq. (17)) a yaw rate estimate is available, reducing the RMSE in the second measurement from 49°/s (*PKF-VD*) to 29°/s. At the third measurement it decreases further to only 11°/s, whereas for the filters without velocity profile the RMSE is constant. More than one second after the initialization, both filters have the same RMSE as with a single velocity profile. The reduced initialization time results in a crucial advantage in detection of hazardous situations, where the target vehicle has a nonlinear motion when it enters the field of view.

C. State Estimation—Example

To evaluate exclusively the tracking performance, the filters are initialized with the ground truth, so that the effects of the previous sections have no effects on the results.

The example of a half-driven figure eight in Fig. 2 is extended to a complete figure eight and the tracking results are shown in Fig. 9. The example consists of two changes in the turning direction, which start at 47.6 s and 54.0 s with a short straight section at 48.1 s and 54.9 s. During this maneuver, there is a clear latency in the yaw rate estimation of *UKF-VD*, which is in the order of 200 ms–1200 ms for the experimental and pre-series radar sensors. The filters using the velocity profile resolve the changing yaw rate without any latency. This is especially surprising for the case with only a single pre-series radar, since a direct estimation of the yaw rate is not possible. There is no significant difference in the yaw rate estimation between the average position and feature based method. *UKF-VD* also shows a larger variability due to the larger process noise. By decreasing the process noise the variability is damped but in return the latency during a yaw rate acceleration increases further. Systematic errors during a constant yaw rate are mainly caused by the relative motion of the average detection on the vehicle.

For the pre-series sensor, the estimation of the velocity and displacement x_S^V estimation are shown in Fig. 10. In both *PKF-VD* and *PKF-VP1*, systematic errors occur due to the relative motion of the representation point on the vehicle. The distance from the average detection to the rear axle varies in this example sequence from -0.5 m up to 3 m, as can be seen from the ground truth in Fig. 10-bottom. Only *FKF-VP* takes this deviation into account and is able to estimate the displacement really precisely without a significant latency. Therefore, the velocity estimation of *FKF-VP* does not underlie systematic variations.

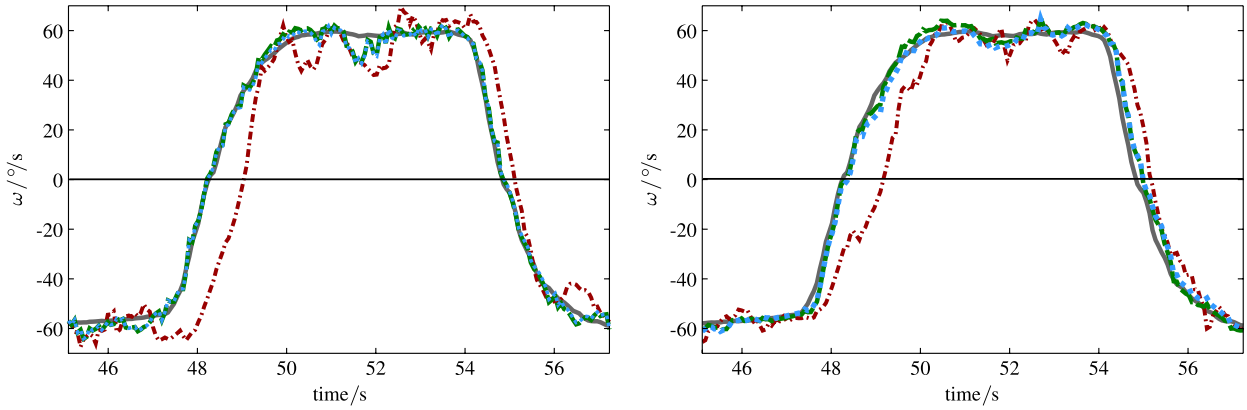

Fig. 9. Example of a driven figure eight in terms of the yaw rate estimation for two experimental (left) and a single pre-series radar (right) for *PKF-VD* (red — · —), *PKF-VP1* (green - - -) and *FKF-VP1* (blue · · ·) compared to the ground truth (gray —) by a highly precise reference system.

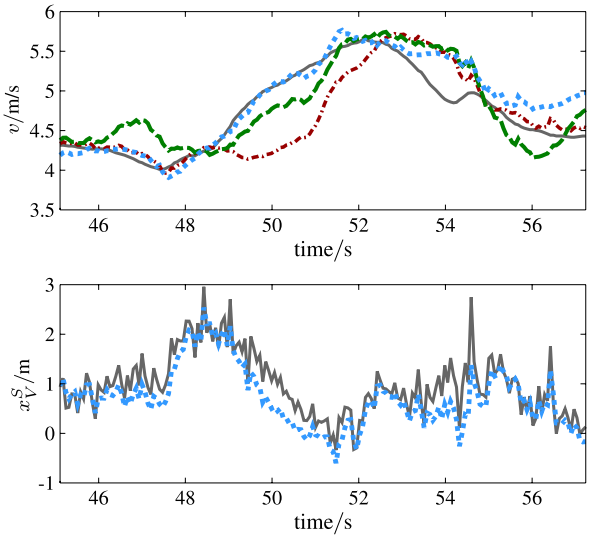

Fig. 10. Sequence from Fig. 9-right for the pre-series radar in terms of velocity estimation (top) and estimation of the displacement x_S^V (bottom) for *PKF-VD* (red — · —), *PKF-VP1* (green - - -) and *FKF-VP1* (blue · · ·) compared to the ground truth (gray —) by a highly precise reference system. x_S^V is only estimated by *FKF-VP1*.

TABLE II
ERROR OF EXAMINED TRACKING FILTERS IN TERMS OF RMSE (MAD) FOR POSITION, HEADING, VELOCITY AND YAW RATE ESTIMATION. ANNOTATION OF FILTER STATES: *PKF* NO ROTATION CENTER ESTIMATION, *FKF* AND *FFKF* ESTIMATION WITH A SINGLE RESPECTIVELY TWO STATES ANNOTATION OF FILTER MEASUREMENTS: *Pos*: POSITION ONLY, *VD*: DOPPLER OF AVERAGE DETECTION, *VP*: VELOCITY PROFILE ANNOTATION OF NUMBER OF SENSORS: *1* RESPECTIVELY *2*

	ϵ(Pos) / m	$\epsilon(\gamma)$ / °	$\epsilon(v)$ / m/s	$\epsilon(\omega)$ / °/s
		Experimental Radar - 1 sensor		
PKF-Pos1	1.61 (1.21)	15.88 (10.20)	0.66 (0.51)	18.62 (9.80)
PKF-VD1	1.49 (1.35)	12.94 (10.50)	0.42 (0.21)	12.43 (6.89)
PKF-VP1	**0.70 (0.60)**	5.82 (3.52)	**0.32 (0.23)**	4.70 (2.29)
FKF-VD1	0.86 (0.76)	9.10 (7.10)	0.40 (0.25)	13.76 (7.04)
FKF-VP1	0.71 (0.60)	**5.80 (3.52)**	0.33 (0.23)	**4.70 (2.28)**
FFKF-VP1	0.85 (0.75)	6.04 (3.66)	0.44 (0.29)	4.67 (2.23)
		Experimental Radar - 2 sensors		
PKF-Pos2	1.60 (1.21)	15.87 (10.12)	0.67 (0.53)	18.74 (9.54)
PKF-VD2	1.58 (1.43)	12.28 (10.27)	0.42 (0.21)	12.57 (7.28)
PKF-VP2	1.19 (0.79)	6.40 (3.96)	0.42 (0.23)	3.72 (1.80)
FKF-VD2	1.44 (1.31)	11.65 (9.66)	0.40 (0.21)	12.21 (7.12)
FKF-VP2	**0.87 (0.68)**	**5.20 (3.36)**	**0.37 (0.20)**	3.72 (1.66)
FFKF-VP2	0.96 (0.79)	5.72 (3.54)	0.46 (0.27)	**3.71 (1.67)**
Instant VP2	- (-)	19.60 (10.39)	1.62 (0.61)	6.43 (3.28)
		Pre-Series Radar - 1 sensor		
PKF-Pos1	1.10 (0.93)	13.66 (8.04)	0.43 (0.32)	20.07 (9.95)
PKF-VD1	1.04 (1.02)	9.81 (7.84)	0.35 (0.20)	13.91 (7.11)
PKF-VP1	1.00 (0.86)	7.34 (5.83)	0.30 (0.19)	4.31 (2.44)
FKF-VD1	0.86 (0.76)	9.10 (7.10)	0.40 (0.25)	13.76 (7.04)
FKF-VP1	**0.71 (0.56)**	**5.46 (3.11)**	**0.25 (0.14)**	**4.31 (2.31)**
FFKF-VP1	0.73 (0.60)	5.47 (3.20)	0.29 (0.19)	4.32 (2.36)

D. State Estimation—Position Based

The 2D position error and the error of the dynamic states are evaluated for all proposed filters and for all sensors on the complete sequence. The results are summarized in Table II. Generally speaking, including the velocity profile improves the accuracy of the yaw rate estimation significantly using either one or two radars. A highly accurate yaw rate estimation is possible with an accuracy up to 3.71°/s, although the scene consists mainly of highly nonlinear maneuvers. The error in the filters using the velocity profile is reduced by a factor of approximately three compared to the integration of the Doppler velocity only (*PKF-VD*) and a factor of four compared to a position tracking only (*PKF-Pos*). The instantaneous estimation with two sensors (*Instant VP2*) shows a promising yaw rate estimation, which is in the same order than a filter approach with a single sensor (*PKF-VP1*).

For the other states of the position based filters, the error decreases less substantially than for the yaw rate and not as consistent over the different sensor configurations. The integration of the velocity profile compared to a Doppler velocity integration reduces the error by 3%–55% for the position, 25%–55% for the heading estimation and 0%–33% for the velocity estimation. For the instant estimation the heading and velocity accuracy is poor. This is caused by the effect that these

values are calculated for the average detection and not at the position of the rear axle, which is unknown.

E. State Estimation—Feature Based

The filters using the velocity profile and with a simultaneous estimation of the x-displacement of the rotation axle (*FKF-VP*), increase the accuracy of the position (27%–46%), heading (22%–34%) and velocity (12%–25%) significantly compared to one without this additional state (*PKF-VP*). As already seen in the example sequence, there is no significant difference in the yaw rate estimation between the position and feature based methods because the yaw rate is independent of the position and mainly estimated by the velocity profiles. The feature based filters shows the best results in all cases.

For the Doppler-only filters (*FKF-VD*) there is no substantial increased accuracy, mainly the errors are shifted marginally between the states and increased. The reason is that with only a Doppler velocity the algorithm is not able to completely resolve the additional state. The same holds for the filters with the 2D-displacement (*FFKF-VP*), the error increases throughout since the two states cannot be resolved substantially by comparing the velocity profile and the position deviation.

F. State Estimation—Sensor Evaluation

Comparing both sensors, the results are slightly more accurate for the pre-series radar, even though it resolves significantly fewer detections from the target. The crucial reason is the highly accurate Doppler velocity estimation, with a measurement uncertainty of factor 6 less than the experimental radar. Comparing both configurations with a single sensor, the pre-series sensor is able to resolve the motion more precisely. An indicator for that is that the additional state (x_S^V) can be better resolved, resulting in a significant increase of the accuracy from *PKF-VP1* to *FKF-VP1*.

Using two Doppler radar sensors results primarily in an increased accuracy in the yaw rate estimation. The other states are almost equal to the single sensor configuration. A potential error is injected due to the requirement for an exact relative calibration between both sensors to perform a common fit of the velocity profile in eq. (11).

VIII. Conclusion

This paper presents an approach to the integration of the Doppler information of multiple detections received from a single target into a tracking algorithm. The approach is evaluated on hand of a large dataset containing ground truth information. The integration of the parameters and corresponding sample variance of the velocity profile improve the yaw rate estimation in particular by a factor of 3 to 4 in a dynamic scenario compared to state-of-the-art approaches. Further, the initialization time of a nonlinear motion state is significantly reduced by at least 700 ms, especially if two Doppler radars receive detections from one target. In an enhancement, a direct integration of the rotation center estimation is presented. Describing the displacement of the rotation center to the average position of the detections increases especially the velocity and heading estimation significantly. The RMSE of the velocity for a single pre-series radar is reduced from 0.40 m/s to 0.25 m/s and of the heading from 9.1° to 5.5°. It has been shown that it is more effective to model the displacement using a single state then using the complete 2D-displacement. By avoiding spatial assumptions on the rotation center (e.g., the rotation center is at the rear axle), the approach is able to handle highly dynamic maneuvers with lateral drift at the rear axle.

References

[1] L. Hammarstrand, L. Svensson, F. Sandblom, and J. Sorstedt, "Extended object tracking using a radar resolution model," *IEEE Trans. Aerosp. Electron. Syst.*, vol. 48, no. 3, pp. 2371–2386, Jul. 2012.

[2] D. Kellner, M. Barjenbruch, J. Klappstein, J. Dickmann, and K. Dietmayer, "Instantaneous full-motion estimation of arbitrary objects using dual Doppler radar," in *Proc. IEEE IV*, Jun. 2014, pp. 324–329.

[3] A. Barth, *Vehicle Tracking and Motion Estimation Based on Stereo Vision Sequences*. München, Germany: Bayerische Akademie der Wissenschaften, 2014.

[4] C. D. Ghilani, *Adjustment Computations: Spatial Data Analysis*. New York, NY, USA: Wiley, 2010.

[5] F. Roos *et al.*, "Estimation of the orientation of vehicles in high-resolution radar images," in *Proc. IEEE MTT-S ICMIM*, Berlin, Germany, 2015, pp. 1–4.

[6] M. Bühren and B. Yang, "Automotive radar target list simulation based on reflection center representation of objects," in *Proc. WIT*, Hamburg, Germany, Mar. 2006, pp. 161–166.

[7] J. Gunnarsson, L. Svensson, L. Danielsson, and F. Bengtsson, "Tracking vehicles using radar detections," in *Proc. IEEE Intell. Veh. Symp.*, Jun. 2007, pp. 296–302.

[8] K. Schuler, D. Becker, and W. Wiesbeck, "Extraction of virtual scattering centers of vehicles by ray-tracing simulations," *IEEE Trans. Antennas Propag.*, vol. 56, no. 11, pp. 3543–3551, Nov. 2008.

[9] D. F. Bizup and D. E. Brown, "Maneuver detection using the radar range rate measurement," *IEEE Trans. Aerosp. Electron. Syst.*, vol. 40, no. 1, pp. 330–336, Jan. 2004.

[10] J. Ru, H. Chen, X. R. Li, and G. Chen, "A range rate based detection technique for tracking a maneuvering target," in *Proc. SPIE Conf. Signal Data Process. Small Targets*, 2005, pp. 1–13.

[11] Z. Duan, X. Rong Li, C. Han, and H. Zhu, "Sequential unscented Kalman filter for radar target tracking with range rate measurements," in *Proc. IEEE 8th Int. Conf. Inf. Fusion*, 2005, vol. 1, pp. 130–137.

[12] S. Zollo and B. Ristic, "On the choice of the coordinate system and tracking filter for the track-while-scan mode of an airborne pulse Doppler radar," Defense Tech. Inf. Center (DTIC) Doc., Belvoir, VA, USA, Tech. Rep., 1999.

[13] B. Kim, K. Yi, H. Yoo, H. Chong, and B. Ko, "An IMM/EKF approach for enhanced multitarget state estimation for application to integrated risk management system," *IEEE Trans. Veh. Technol.*, vol. 64, no. 3, pp. 876–889, Mar. 2015.

[14] C. Yang, W. Garber, R. Mitchell, and E. Blasch, "A simple maneuver indicator from targets range-Doppler image," in *Proc. IEEE 10th Int. Conf. Inf. Fusion*, 2007, pp. 1–8.

[15] R. Fitzgerald, "Effects of range-Doppler coupling on chirp radar tracking accuracy," *IEEE Trans. Aerosp. Electron. Syst.*, vol. AES-10, no. 4, pp. 528–532, Jul. 1974.

[16] W. K. Yan and Y. C. Lap, "Fast rotation center identification methods for video sequences," in *Proc. IEEE Int. Conf. Multimedia Expo*, 2005, pp. 289–292.

[17] W. A. Fuller, *Measurement Error Models*, vol. 305. New York, NY, USA: Wiley, 2009.

[18] P. T. Boggs, R. H. Byrd, and R. B. Schnabel, "A stable and efficient algorithm for nonlinear orthogonal distance regression," *SIAM J. Sci. Statist. Comput.*, vol. 8, no. 6, pp. 1052–1078, 1987.

[19] E. A. Wan and R. Van Der Merwe, "The unscented Kalman filter for nonlinear estimation," in *Proc. IEEE Adaptive Syst. Signal Process., Commun., Control Symp.*, 2000, pp. 153–158.

[20] M. Arulampalam, S. Maskell, N. Gordon, and T. Clapp, "A tutorial on particle filters for online nonlinear/non-Gaussian Bayesian tracking," *IEEE Trans. Signal Process.*, vol. 50, no. 2, pp. 174–188, Feb. 2002.

[21] A. Doucet, N. De Freitas, K. Murphy, and S. Russell, "Rao-Blackwellised particle filtering for dynamic Bayesian networks," in *Proc. 16th Conf. Uncertainty Artif. Intell.*, San Francisco, CA, USA, 2000, pp. 176–183.

[22] X. R. Li and V. P. Jilkov, "Survey of maneuvering target tracking. Part I. Dynamic models," *IEEE Trans. Aerosp. Electron. Syst.*, vol. 39, no. 4, pp. 1333–1364, Oct. 2003.
[23] Y. Bar-Shalom, X. R. Li, and T. Kirubarajan, *Estimation With Applications to Tracking and Navigation: Theory Algorithms and Software*. New York, NY, USA: Wiley, 2004.

Dominik Kellner (S'15) was born in Munich, Germany in 1985. He received the Dipl.Ing. degree (equivalent to M.Sc. degree) in mechatronics and information technology from the Technische Universität München, Munich, in 2010. He is currently working toward the Ph.D. degree at Ulm University, Ulm, Germany.

His research interests include automotive radar and environmental perception with a focus on motion state estimation of extended objects. Further research topics are radar alignment and ego-motion state estimation using high-resolution Doppler radar.

Michael Barjenbruch (S'15) was born in Hannover, Germany in 1986. He received the Dipl.Ing. degree in electrical engineering from Leibniz University, Hannover, Germany, in 2011. He is currently working toward the Ph.D. degree at Ulm University, Ulm, Germany.

His research interests include radar signal processing and vehicle environment perception.

Jens Klappstein received the Diploma degree in computer science from the Technical University of Ilmenau, Ilmenau, Germany, in 2004 and the Ph.D. degree in computer science from Heidelberg University, Heidelberg, Germany, in 2008. Since 2004, he has been with Daimler AG, Ulm, Germany. His research interests are high-resolution digital beamforming algorithms and tracking algorithms of extended objects.

Jürgen Dickmann received the Diploma degree in electrical engineering from the University of Duisburg, Duisburg, Germany, in 1984 and the Dr.-Ing. degree from the Rheinisch Westfaelische Technische Hochschule (RWTH) Aachen University, Aachen, Germany, in 1991. He is the Active Sensors Manager with Daimler Research and Advanced Engineering, Ulm, Germany. He is responsible for the development of active sensors and environmental perception in driver assistance and active-safety systems. His present focus is in sensor technology such as 76-GHz radar, lidar, and laser scanner technology for highly automated driving functions. In 1992, he was an awardee from VDE/ITG. In 1986, he started his career at the AEG Research Center, Ulm, where he conducted research on III/V processing techniques, millimeter-wave devices, and monolithic microwave integrated circuits. Between 2005 and 2009, he was in charge of teams developing sensor technologies, sensor fusion, and situation analysis concepts.

Klaus Dietmayer (M'05) was born in Celle, Germany in 1962. He received the Diploma degree (equivalent to M.Sc. degree) in electrical engineering from Braunschweig University of Technology, Braunschweig, Germany, in 1989 and the Dr.-Ing. degree (equivalent to Ph.D. degree) from the Helmut Schmidt University, Hamburg, Germany, in 1994. In 1994, he joined the Philips Semiconductors Systems Laboratory, Hamburg, as a Research Engineer. Since 1996, he has been a Manager in the field of networks and sensors for automotive applications. In 2000, he was appointed to a professorship at Ulm University, Ulm, Germany, in the field of measurement and control. He is currently a Full Professor and the Director of the Institute of Measurement, Control and Microtechnology with the School of Engineering and Computer Science, Ulm University. His research interests include information fusion, multiobject tracking, environment perception for advanced automotive driver assistance, and E-Mobility.

Dr. Dietmayer is a member of the German Society of Engineers VDI/VDE.